Journal of Biomedical Optics

SPIEDigitalLibrary.org/jbo

From supersonic shear wave imaging to full-field optical coherence shear wave elastography

Amir Nahas
Mickaël Tanter
Thu-Mai Nguyen
Jean-Marie Chassot
Mathias Fink
A. Claude Boccara

SPIE

From supersonic shear wave imaging to full-field optical coherence shear wave elastography

Amir Nahas,* Mickaël Tanter, Thu-Mai Nguyen, Jean-Marie Chassot, Mathias Fink, and A. Claude Boccara
Institut Langevin, ESPCI-ParisTech, CNRS UMR7587, INSERM U979, 1 rue Jussieu, Paris 75005, France

Abstract. Elasticity maps of tissue have proved to be particularly useful in providing complementary contrast to ultrasonic imaging, e.g., for cancer diagnosis at the millimeter scale. Optical coherence tomography (OCT) offers an endogenous contrast based on singly backscattered optical waves. Adding complementary contrast to OCT images by recording elasticity maps could also be valuable in improving OCT-based diagnosis at the microscopic scale. Static elastography has been successfully coupled with full-field OCT (FF-OCT) in order to realize both micrometer-scale sectioning and elasticity maps. Nevertheless, static elastography presents a number of drawbacks, mainly when stiffness quantification is required. Here, we describe the combination of two methods: transient elastography, based on speed measurements of shear waves induced by ultrasonic radiation forces, and FF-OCT, an *en face* OCT approach using an incoherent light source. The use of an ultrafast ultrasonic scanner and an ultrafast camera working at 10,000 to 30,000 images/s made it possible to follow shear wave propagation with both modalities. As expected, FF-OCT is found to be much more sensitive than ultrafast ultrasound to tiny shear vibrations (a few nanometers and micrometers, respectively). Stiffness assessed in gel phantoms and an *ex vivo* rat brain by FF-OCT is found to be in good agreement with ultrasound shear wave elastography. [DOI: 10.1117/1.JBO.18.12.121514]

Keywords: optical coherence tomography; elastography; shear wave imaging; cancer diagnosis.

Paper 130455SSRR received Jul. 1, 2013; revised manuscript received Nov. 27, 2013; accepted for publication Dec. 2, 2013; published online Dec. 19, 2013.

1 Introduction

Human tissue exhibits intrinsic mechanical properties that often differ between healthy and pathological states.[1] Adding an elastography map to morphological or functional images has been shown to be a valuable aid to cancer diagnosis when using MRI[2] or ultrasonic imaging.[3] Since the pioneering work of Schmitt[4] combining optical coherence tomography (OCT) and elastography, a number of static or dynamic approaches have been proposed for optical coherence elastography in two- or three-dimensional (3-D).[5–10] In these previous studies, only compressive waves were used. More recently, shear waves have been coupled to OCT.[11]

Stiffness imaging based on the ultrasonic imaging of tissue deformations induced by a quasistatic compression of organs was first introduced in the early 1990s by Ophir et al. and named elastography.[12] Tissue deformation information is obtained by acquiring two "precompression" and "postcompression" ultrasonic images of the organ using a conventional ultrasound scanner. This static method suffers, however, from some major drawbacks. The strain distribution image is linked to stiffness since soft regions tend to exhibit a higher strain than stiffer areas. Unfortunately, applying a quasistatic compression at the surface of the sample can create a very complex spatial distribution of stress that both prevents the quantitative assessment of local stiffness and induces image artifacts. The Young's modulus E can be strongly biased by the unknown local stress according to Hooke's law $E = \tau/\zeta$, where τ and ζ are, respectively, the local stress and strain.

For homogeneous and isotropic tissues, Young's modulus can be expressed by two parameters:

$$E = \frac{9K\mu}{3K + \mu}, \tag{1}$$

where K and μ are the bulk and shear moduli, respectively. K is the inverse of the compressibility.

For soft biological tissues, $K \gg \mu$, leading to

$$E = 3\ \mu. \tag{2}$$

The great difference between K and μ can also be seen as a great difference between the compression wave speed (typically 1540 m/s for soft biological tissues) and the shear wave speed (a few m/s). Ultrasound structural images are based on compression waves, i.e., their contrast is related to the bulk modulus, whereas elastography images are based on shear modulus contrast.

Stiffness can be accessed through the shear wave speed c_s that depends on the "local" shear modulus μ and on the local density ρ

$$c_s = \sqrt{\mu/\rho}. \tag{3}$$

Combined with Eq. (2), this yields the fundamental equation of dynamic elastography in homogeneous, isotropic, and incompressible tissues

$$E = 3\ \rho c_s^2. \tag{4}$$

It should be noted that in particular cases such as shear wave propagation in soft plates with a thickness less than the shear

*Address all correspondence to: Amir Nahas, E-mail: amir.nahas@espci.fr

0091-3286/2013/$25.00 © 2013 SPIE

wavelength, Eq. (3) is no longer valid, as the propagation regime corresponds in such cases to a leaky Lamb wave.[13]

Dynamic elastography methods consist of two steps: first, a shear wave is induced in the sample; then, the shear wave propagation is imaged. Different ultrasound-based techniques have been developed for medical applications.[14–16] Our group has previously developed a technique called supersonic shear wave imaging, using the ultrasound radiation force to create short shear impulses and ultrasound ultrafast imaging to image the shear wave propagation.[17,18] Very high frame rates are required to properly sample the shear wave propagation. Our group has developed such an ultrafast scanner (Aixplorer®, Supersonic Imaginig, Aix-en-Provence, France)[18] emitting plane waves to insonicate a wide area covering the whole region of interest. Backscattered echoes are then digitally beamformed to retrieve an echographic image. This allows to reach frame rates >10,000 frames/s.

Here, we demonstrate that the full-field optical coherence tomography (FF-OCT) method, that offers micrometer-scale resolution, and is able to perform measurements of the local shear wave velocity through optically scattering samples, thereby opening up the possibility for Young's modulus determination at the micrometer scale.

More precisely, we describe the experimental setup leading to the dynamic multiwave method we have developed in order to add an elastographic contrast to a FF-OCT image.

Interestingly, ultrafast scanners (1 to 20,000 frames/second) were initially introduced in the medical ultrasound community in order to track shear waves for quantitative elastography imaging in order to overcome the drawbacks of static elastography. Here, we propose a similar approach in the optical domain. FF-OCT performed with ultrafast camera technology is used to track shear waves at similar frame rates but smaller spatial scales. FF-OCT shear wave imaging corresponds to a multiwave imaging approach[19] giving access to the shear modulus contrast at OCT-scale resolution.

2 Experimental Setup Combining FF-OCT and Ultrasonically Generated Shear Waves

2.1 *Shear Wave Generation*

Shear waves were induced using a programmable ultrasound scanner (Aixplorer®, Supersonic Imaginig, Aix-en-Provence, France), initially developed by our group for ultrasound-based shear wave imaging purposes. A 15-MHz ultrasound linear array (128 elements, pitch 100 μm, elevation focus at 12 mm, Vermon, France) was used to focus ultrasonic "pushing" beams for tens of microseconds in the sample. The resulting radiation force remotely creates a controlled shear source in the sample, as proposed by Sarvazyan et al.[20] This force is localized in the ultrasound focal spot and oriented along the beam axis. It is due to the momentum transfer from the ultrasonic wave to the medium caused by the damping of the ultrasonic power.

The tissue relaxation that follows the application of the radiation force generates a shear wave that is polarized along the ultrasonic beam and propagates transversally to the ultrasonic beam.

However, shear waves radiating from a single focal spot are rapidly attenuated due to the divergence associated with spatially limited shear sources. To increase the amplitude of the radiated shear wave, quasi-planar shear waves were induced using the supersonic shear source generation implemented on the Aixplorer®. This original solution consists of successively focusing the ultrasonic beams at different depths along the ultrasonic path. Thus, the shear source is moved at a higher speed than the speed of the radiated shear wave, inducing constructive interference along a Mach cone (Fig. 1). The resulting shear wave can propagate with minimized diffraction over a large area.

For short ultrasonic bursts (shorter than 1 millisecond), the spatial distribution of large tissue displacements initially corresponds to the acoustic intensity distribution, i.e., a cylinder with a lateral extension of 200 μm and an axial extension of about 1 mm in our configuration.

The use of a linear array provides great flexibility in the location of the shear source. The shear source can be swept by electronically focusing the ultrasound beam at different lateral locations, without any mechanical translation involved.

The pressure levels involved are within the limits set by the Food and Drug Administration (FDA) for the application of diagnostic ultrasound in most organs (breast, liver, kidney, peripheral vasculature).

2.2 *FF-OCT Imaging System*

Our FF-OCT system is based on a Linnik interferometer (Fig. 2).[21–23] The halogen source uses a Kohler illuminator to ensure homogeneous illumination of the sample. As the spectrum of the halogen source is broad, we used two filters: a high-pass filter at 610 nm and a low-pass filter at 1000 nm in order to avoid unnecessary heating of the sample. Taking into account the spectral response of the camera, the effective spectral bandwidth equals 200 nm, centered around 710 nm.

In each arm of the interferometer, we placed an identical water-immersion microscope objective (Olympus, 10×, NA = 0.3). In the reference arm, we used a barium titanate wafer mirror (reflectivity of about 7%). We recorded the images

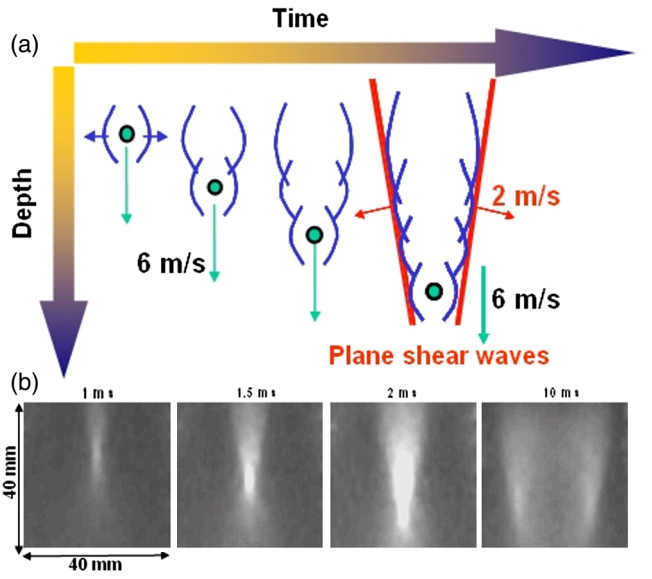

Fig. 1 Generation of a supersonic shear source. (a) Bursts of ultrasound are focused at successive depths in the organ. Each burst creates "pushing" radiation force at focus that induces a shear wave. As the "pushing" force is moved faster than the shear waves, it generates, a supersonic regime is reached and shear waves accumulate on a Mach cone. (b) Images (40×40 mm^2) of micrometric displacements induced in a tissue-mimicking phantom obtained using the ultrasonic ultrafast imaging mode at different time steps (from Ref. 16).

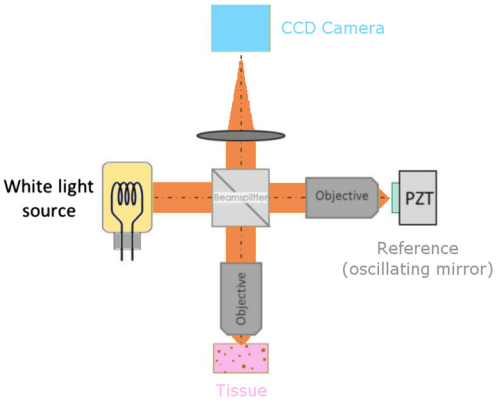

Fig. 2 Schematic representation of the full-field optical coherence tomography (FF-OCT) setup. For clarity, only one voxel of the sample interfere with one pixel of the reference plane is represented; the ultrafast camera used here allows parallelization of 1 megapixel signals.

with an ultrafast camera (Vision Research Phantom V12, 1024×1024 pixels at 10,000 Hz or 512×255 pixels at 30,000 Hz, 12 bits, full well capacity of 20 000 e^-).

With this custom setup, we achieved lateral resolution of 1.4 μm and axial resolution of 1 μm with sensitivity of >60 dB (for a single image acquisition).

As illustrated in Fig. 3, the ultrasound probe was placed underneath of the sample, while the FF-OCT objective was facing the top of the sample. By synchronizing the ultrasonic push with image acquisition by the CCD camera, we were able to record the propagation of the shear wave, i.e., to record the local displacement along the z-axis induced by the shear wave propagation.

3 Shear Wave Detection Using FF-OCT and Shear Modulus Estimation

3.1 *Shear Wave Detection Using FF-OCT*

By considering the manner in which the signal is generated, we can evaluate the sensitivity of the approach. The signal I_0 on each pixel of the camera can be written as

$$I = I_0 \{1 + a_\delta \cos[2\pi\delta\sigma + \phi(t)]\}, \tag{5}$$

where a_δ is linked to the backscattered wave amplitude interfering with the reference signal, δ is the path length difference at the pixel of interest, σ is the central wave number of light, and $\phi(t)$ is the time-dependent phase variation associated with the displacements of the local scatterers induced by the shear wave. As previously mentioned, displacements of the order of the optical wavelength can be induced with an acoustic power much lower than the limits recommended by the FDA. This means that the signals are expected to reach the usual FF-OCT level, as the usual path modulation induced by the piezoelectric ceramic in the sample arm (Fig. 2) is replaced by an internal sample path modulation.

From the movie of the shear wave propagation, we calculate the temporal cross-correlation between neighboring pixels. From the cross-correlation calculation, we obtain the time delay, and hence the local shear wave speed.

In order to visualize the propagation of the mechanical perturbation, we subtract the average of the frames captured before the generation of the acoustic push from the whole movie. The signal before the mechanical perturbation I_{ini} on each camera pixel can be expressed as

$$I_{\text{ini}} = I_0 [1 + a_\delta \cos(2\pi\delta\sigma + \varphi_{\text{ini}})], \tag{6}$$

where φ_{ini} is the initial phase.

By subtracting the initial image from all images of the time-dependent signal, a signal I_{diff} can be obtained as

$$I_{\text{diff}} = I_0.a_\delta [\cos(2\pi\delta\sigma + \varphi(t)] - \cos[2\pi\delta\sigma + \varphi_{\text{ini}})]. \tag{7}$$

The signal in this new movie is directly proportional to the cosine of the phase. In Sec. 4, the images shown are the absolute value of frames from this movie.

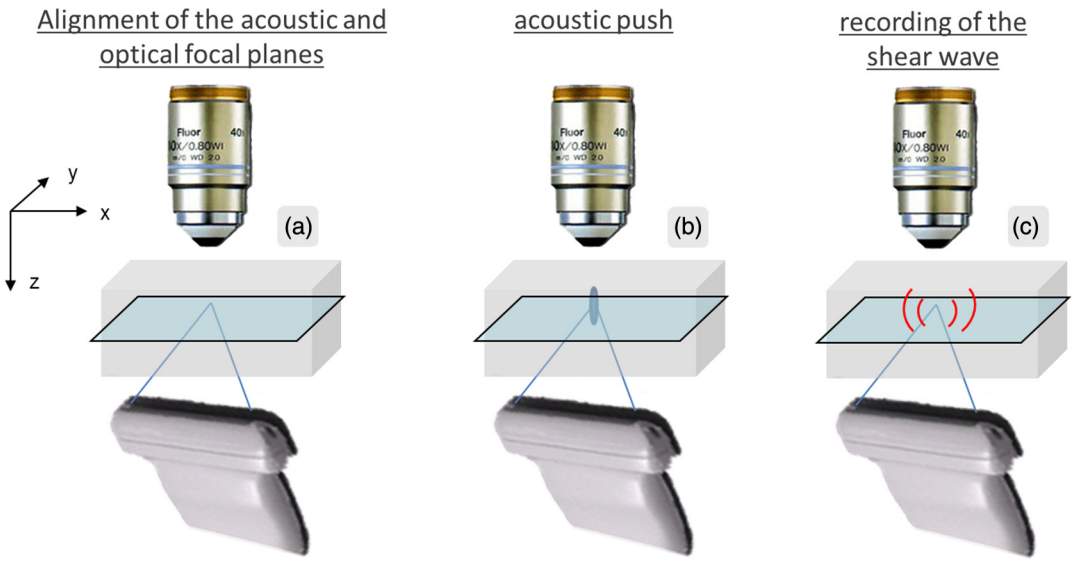

Fig. 3 Schematic illustrating the principle of combining FF-OCT and ultrasonically generated shear waves. (a) First, both acoustic and optical focal plans are aligned. (b) Then by focusing compression waves emitted by the transducer array, a shear wave polarized along the z axis is generated. (c) Finally, the propagation of the shear wave is recorded with the FF-OCT system.

3.2 *Shear Modulus Estimation*

With the method just described, we were able to detect axial displacements with a sensitivity of about 10 nm. However, the measurements presented here show a major difference from the ultrasonic setup. With FF-OCT, we typically probe the top 200 μm of the biological tissues, so we are not only looking at volumetric waves but also at surface waves. At a solid/liquid interface, as is the case here between the sample and the silicon immersion oil used as an optical coupler, we observe shear waves perturbed by the surface that are called Scholte waves.[24]

To our knowledge, there is no easy analytical expression of the Scholte wave speed. In order to verify that what we measured is still linked to the stiffness of the sample, we used a finite difference algorithm developed by Bossy.[25] Using this algorithm based on the De Virieux scheme, we were able to simulate our experiment. The total size of the simulation was 2×2 mm^2 with a spatial grid step of 1 μm, a temporal grid step of 1 μs, and absorbing boundaries conditions (perfectly matched layers). We first verified that with a transducer of 15 MHz, the Scholte wave dominates in the first 200 μm of the sample. We also showed that for stiffnesses comparable to those found in the human body (shear wave speeds from 1 to 10 m/s), there is quite a straightforward relationship between the Scholte wave speed and the shear wave speed. Figure 4(a) shows a plot of shear wave and Scholte wave speeds as a function of the simulated stiffness, whereas Fig. 4(b) shows the ratio between the Scholte and the shear wave speeds. From these simulations, we can develop the following relationship between the Scholte (v_{Scholte}) and the shear (v_s) wave speeds as

$$v_{\text{Scholte}} = 0.664 \times v_s + 0.01 \times v_s^2. \tag{8}$$

This equation is verified by simulations with less than 2% error. From Scholte wave speed measurements, we were able to deduce the volumetric shear wave speed, and in doing so access the shear modulus μ.

4 Results

4.1 *Proof of Principle on a Phantom*

The method was first tested on optically and mechanically homogeneous samples.

The first sample was made of polyvinyl alcohol (PVA-341584, Sigma-Aldrich, Saint Louis, Missouri) and silver particles from a silver paint (PEBEO-Colorex: silver-342048, Gemenos, France). Stiffness of PVA samples can be tuned by the number of freezing cycles. Here, we applied two freezing cycles with a sample made of 5% of PVA.

Figure 5(a) shows a standard FF-OCT image of the sample using classic four phase imaging.[21] Images at different time points of the propagation are shown in Figs. 5(b)–5(d). This recording was performed at 10 kHz with 1024×1024 pixels and an exposure time of 30 μs.

The second sample was made of agarose (Agarose-A9539, Sigma-Aldrich, Saint Louis, Missouri) and zinc oxide (ZnO-205532, Sigma-Aldrich, Saint Louis, Missouri) particles. ZnO particles were selected to induce optical scattering while the agarose concentration controls the stiffness of the sample.

With a ZnO particle concentration of 0.2 mgg^{-1} and an agarose concentration of 1%, we acquired the images at 30 kHz with 512×255 pixels and an exposure time of 30 μs.

For these two samples, we measured the shear wave speed with an ultrasound system and the Scholte wave speed with our fast FF-OCT system at 10 μm beneath the surface.

Table 1 presents the results obtained. We observe that there is a good correlation between the values obtained with the ultrasound system and the FF-OCT system.

4.2 *Ex Vivo Biological Tissues*

As the final objective of this study is to aid medical diagnosis by complementing the FF-OCT images with quantitative stiffness information, a preliminary result on *ex vivo* rat brain in the

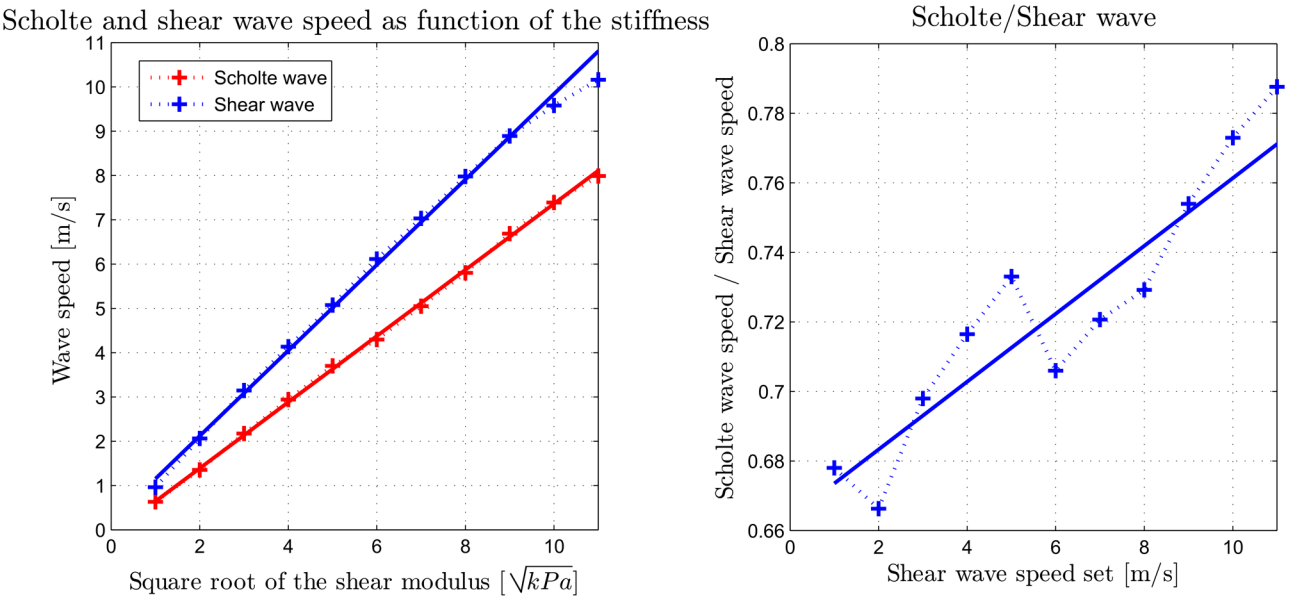

Fig. 4 Simulation results of the propagation speed of volumetric shear and Scholte waves in isotropic media of different stiffnesses. (a) Volumetric shear and Scholte wave speeds as functions of the square root of the shear modulus $\sqrt{\mu}$. (b) Ratio between the Scholte wave speed and the volumetric shear wave speed as a function of the square root of the shear modulus $\sqrt{\mu}$.

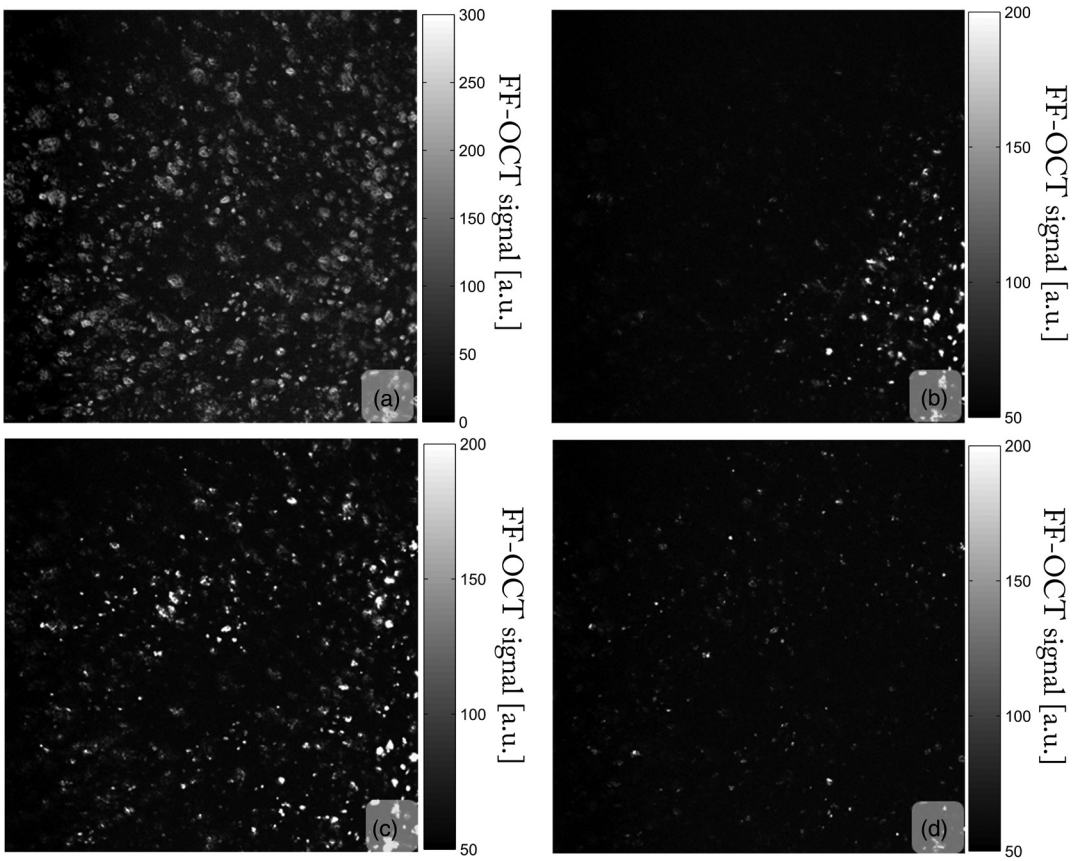

Fig. 5 Images of a PVA-silver particle sample recorded at 10,000 Hz with a field of view of $950 \times 950\ \mu m^2$. (a) Classic four-phase FF-OCT image of the sample. Silver particles vary considerably in size. (b)–(d) are frames from a movie of the wave propagation corresponding to $t_b = 100$ ms, $t_c = 300$ ms and $t_d = 800$ ms, respectively.

frontal lobe cortex was obtained. For this experiment, we used the whole brain.

Figure 6(a) shows a standard FF-OCT image of the *ex vivo* rat brain. Images at different time points of the propagation are shown in Figs. 6(b)–6(e). Figure 6(f) shows the arrival time of the acoustic wavefront at different positions along the x axis. For each position, the signal is averaged along the y axis. We can see that the farther we are from the source, the longer the arrival time is. This recording was performed at 30 kHz with 512×255 pixels and an exposure time of 30 μs.

Table 1 Results obtained on the PVA-silver and agarose-ZnO samples. The shear wave speed corresponding to the Scholte wave speed measured with the FF-OCT system was calculated using Eq. (5).

	Scholte wave speed measured with the FF-OCT system (m/s)	Shear wave speed measured with the ultrasound system (m/s)	Shear wave speed corresponding to the Scholte wave speed measured with the FF-OCT system (m/s)
PVA-silver	1.2	1.5 ± 0.2	1.77
Agarose-ZnO	3.95	5.0 ± 0.2	5.6

From the movie of the Scholte wave propagation, we measure a Scholte wave speed of 0.43 ms^{-1} corresponding to a shear modulus of 0.41 kPa. This value of the shear modulus is quite low; it corresponds well with the literature for values obtained in *ex vivo* rat brain using MR-elastography[26] as well as supersonic shear wave imaging.[27]

5 Discussion and Conclusion

To the best of our knowledge, we have presented the first combination of an FF-OCT setup with an ultrafast camera for real-time 2-D tracking of shear wave propagation. We have been able to follow the instantaneous shear wave propagation and measure the wave velocity that is directly linked to the local stiffness of the sample. In parallel, we are working on static elastography combined with FF-OCT.[28] This approach provides valuable imaging contrast but, as previously mentioned, is not able to provide quantitative information related to the stiffness.

For this purpose, we have built an FF-OCT setup that can function at speeds of 10,000 to 30,000 images/s. This places it in the gigapixels/s range, a few hundred times faster than the commercial OCT systems. The setup was easily synchronized with a commercial ultrasonic system (Aixplorer®, Supersonic Imaginig, Aix-en-Provence, France).

The signal-to-noise ratio was high enough to work on various phantoms of different stiffnesses and with *ex vivo* biological tissue. The ultrasound scanner was able to track shear waves from ultrasonic radiation force "pushes" generating displacements of

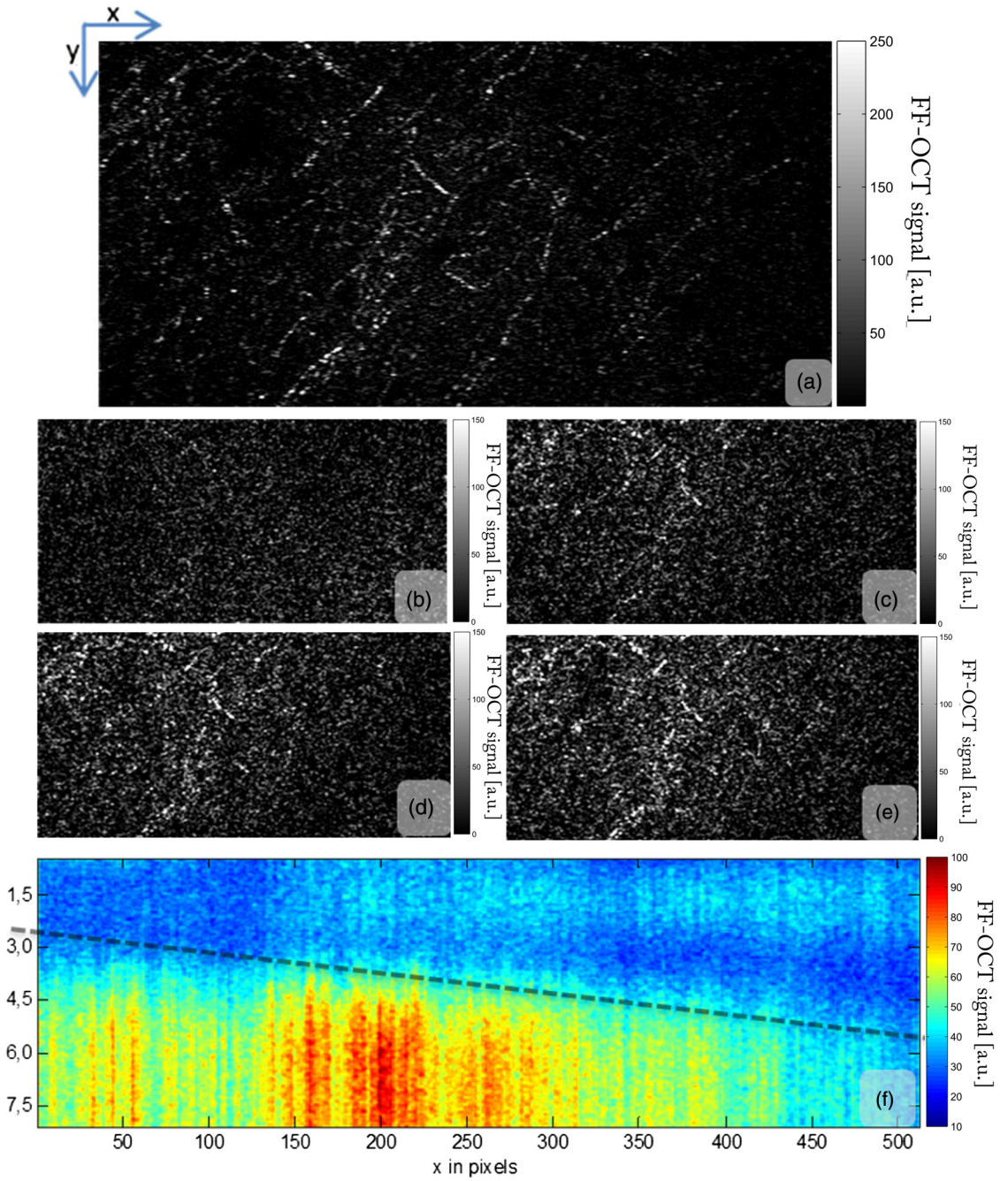

Fig. 6 Images of an *ex vivo* rat brain recorded at 30,000 Hz with a field of view of 471×235 μm. (a) Standard four-phase FF-OCT image of the sample. (b)–(e) are frames from a movie of the wave propagation corresponding to $t_b = 0$ ms, $t_c = 0.6$ ms, $t_d = 1.2$ ms and $t_e = 1.8$ ms, respectively. (f) is the plot of the temporal evolution of the average image intensity along the y axis.

several micrometers, whereas FF-OCT was able to detect and track shear waves from much lower acoustic intensities (more than twofold). This is of particular interest, for example, in the field of corneal elasticity mapping, for which the FDA requirements in terms of acoustic deposit are very restrictive.

Although our images exhibit the standard resolution of the FF-OCT setup (typically 1 μm in 3-D), one should bear in mind that the determination of spatial resolution is a very complex problem and we intend to work toward a better understanding of the spatial resolution in order to improve it for further studies.

Our measurement of the speed of the shear wave consisted of detecting the arrival of the pulse generated by the ultrasound "push" on each pixel by carrying out a time correlation.

Figure 7 shows the time dependence of the detected signal for one pixel for the *ex vivo* rat brain experiment. As expected, its rise time is determined by the shear wave speed and the transverse dimension of the source (here about 200 μm). The determination of the time corresponding to the arrival of the acoustic wave is linked to this rise time, the signal-to-noise ratio of the pixels on which we calculated the correlation, and the sampling rate (camera frame rate).

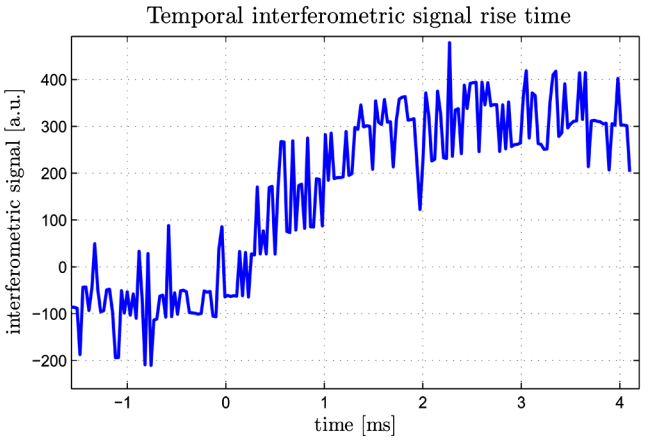

Fig. 7 Time variation of the interferometric signal for one voxel from the experiment on *ex vivo* rat brain.

As the signal-to-noise ratio depends directly on the FF-OCT signal and is different for each pixel, it is very difficult to calculate the characteristic spatial sensitivity of detection for the whole image.

For example, in the case of the *ex vivo* rat brain, for a signal level corresponding to the pixel shown in Fig. 7, we are able to experimentally estimate an approximate spatial sensitivity. With a camera frame rate of 30 kHz, a rise time of about 2 ms and the signal level shown in Fig. 7, we approximately estimate the smallest measurable time delay to be 150 ms. As the wave speed is 0.43 m/s, this corresponds to a spatial sensitivity of about 65 μm.

Up to now, the main limitation is the camera frame rate that limits the speed of the shear wave that can be recorded. To overcome this limitation and improve the signal-to-noise ratio, we are currently working on implementing a stroboscopic approach.

Nevertheless, the aim of stiffness measurements is to aid physicians with their diagnoses by complementing the FF-OCT-based tissue characterization. We intend to perform experiments on fresh pathological tissues, such as breast cancer tumors, and to correlate the results with histology slides. Finally, FF-OCT combined with the ultrasonic radiation force represents a first step toward quantitative elastography of biological samples at the micrometric scale.

Acknowledgments

We would like to thank Fabien Mézière, PhD student at Institut Langevin, Paris (France), for his help and advice on the numerical simulations; Jean Luc Gennisson, from Institut Langevin, Paris (France), for support in using the Aixplorer system; Fabrice Harms, Anne Latrive, Franck Martins, Charles Brossollet, Kate Grieve, and Eugenie Dalimier, members of LLTech, Paris (France), for technical support and advice; and Armelle Rancillac and Delphine Ladarré from the Neurobiology Laboratory, ESPCI-ParisTech, Paris (France), for providing the excised samples. This research has been supported by the INSERM program DESP – Physique – Mathématiques – Sciences ingénieurs et Cancer and by LABEX WIFI (Laboratory of Excellence within the French Program "Investments for the Future") under references ANR-10-LABX-24 and ANR-10-IDEX-0001-02 PSL. Conflict of interest: M. F. and M. T. are co-founders and shareholders of Super Sonic Imagine. C. B. is co-founder and shareholder of LLTech that manufactures the Light-CT scanner and A. N. receives funding for his doctoral studies from LLTech. Super Sonic Imagine and LLTech did not sponsor the current study.

References

1. A. Sarvazyan, "Shear acoustic properties of soft biological tissues in medical diagnostics," *J. Acoust. Soc. Am.* **93**(4), 2329–2330 (1993).
2. Y.K. Mariappan, K.J. Glaser, and R.L. Ehman, "Magnetic resonance elastography: a review," *Clin. Anat.* **23**, 497–511 (2010).
3. M. Tanter et al., "Quantitative assessment of breast lesion viscoelasticity: initial clinical results using supersonic shear imaging," *Ultrasound Med. Biol.* **34**(9), 1373–1386 (2008).
4. J. Schmitt, "OCT elastography: imaging microscopic deformation and strain of tissue," *Opt. Express* **3**(6), 199–211 (1998).
5. C. Sun, B. Standish, and V. X. D. Yang, "Optical coherence elastography: current status and future applications," *J. Biomed. Opt.* **16**(4), 043001 (2011).
6. A. S. Khalil et al., "Tissue elasticity estimation with optical coherence elastography: toward mechanical characterization of in vivo soft tissue," *Ann. Biomed. Eng.* **33**(11), 1631–1639 (2005).
7. R. K. Wang, S. Kirkpatrick, and M. Hinds, "Phase-sensitive optical coherence elastography for mapping tissue microstrains in real time," *Appl. Phys. Lett.* **90**(16), 164105 (2007).
8. R. K. Wang, Z. Ma, and S. J. Kirkpatrick, "Tissue Doppler optical coherence elastography for real time strain rate and strain mapping of soft tissue," *Appl. Phys. Lett.* **89**(14), 144103 (2006).
9. X. Liang, V. Crecea, and S. A. Boppart, "Dynamic optical coherence elastography: a review," *J. Innov. Opt. Health Sci.* **3**(4), 221–233 (2010).
10. B. F. Kennedy et al., "*In vivo* three-dimensional optical coherence elastography," *Opt. Express* **19**(7), 6623–6634 (2011).
11. M. Razani et al., "Feasibility of optical coherence elastography measurements of shear wave propagation in homogeneous tissue equivalent phantoms," *Biomed. Opt. Express* **3**(5), 972–980 (2012).
12. J. Ophir et al., "Elastography: a quantitative method for imaging the elasticity of biological tissues," *Ultrasonic Imaging* **13**(2), 111–134 (1991).
13. T.-M. Nguyen et al., "Assessment of viscous and elastic properties of sub-wavelength layered soft tissues using shear wave spectroscopy: theoretical framework and in vitro experimental validation," *IEEE Ultrasound Ferro. Freq. Control* **58**(11), 2305–2315 (2011).
14. K. Nightingale et al., "Acoustic radiation force impulse imaging: in vivo demonstration of clinical feasibility," *Ultrasound Med. Biol.* **28**, 227–235 (2002).
15. M. Fatemi and J. F. Greenleaf, "Ultrasound-stimulated vibro-acoustic spectrography," *Science* **280**, 82–85 (1998).
16. J. Bercoff, M. Tanter, and M. Fink, "Supersonic shear imaging: a new technique for soft tissue elasticity mapping," *IEEE Ultrasound Ferroelectr. Freq. Control* **51**(4), 396–409 (2004).
17. S. Catheline et al., "Diffraction field of a low frequency vibrator in soft tissues using transient elastography," *IEEE Ultrasound Ferroelectr. Freq. Control* **46**(4), 1013–1019 (1999).
18. L. Sandrin et al., "Time resolved pulsed elastography with ultrafast ultrasonic imaging," *IEEE Ultrasound Ferroelectr. Freq. Control*, **49**(4), 426–435 (2002).
19. M. Fink and M. Tanter," Multiwave imaging and superresolution," *Phys. Today* **63**(2), 28–33 (2010).
20. A.P. Sarvazyan et al., "Shear wave elasticity imaging - a new ultrasonic technology of medical diagnostic," *Ultrasound Med. Biol.* **24**(9), 1419–1436 (1998).
21. E. Beaurepaire et al., "Full-field optical coherence microscopy," *Opt. Lett.* **23**(4), 244–246 (1998).
22. A. Dubois et al., "Ultrahigh-resolution full-field optical coherence tomography," *Appl. Opt.* **43**, 2874–2883 (2004).
23. K. Grieve et al., "Ultrahigh resolution ex vivo ocular imaging using ultrashort acquisition time en face optical coherence tomography," *J. Opt. A Pure Appl. Opt.* **7**(8), 368–373 (2005).
24. A. N. Norris and B. K. Sinha, "The speed of a wave along a fluid/solid interface in the presence of anisotropy and prestress," *J. Acoust. Soc. Am.* **98**(2), 1147–1154 (1995).
25. E. Bossy, M. Talmant, and P. Laugier, "Three-dimensional simulations of ultrasonic axial transmission velocity measurement on cortical bone models," *J. Acoust. Soc. Am.* **115**, 2314–2324 (2004).

26. S. Chatelin, A. Constantinesco, and R. Willinger, "Fifty years of brain tissue mechanical testing: from in vitro to in vivo investigations," *Biorheology* **47**(5–6), 255–276 (2010).
27. E. Mace et al.," *In vivo* mapping of brain elasticity in small animals using shear wave imaging," *IEEE Trans. Med. Imaging* **30**(3), 550–558 (2011).
28. A. Nahas et al., "3D static elastography using full field OCT," *Biomed. Opt. Express* **4**(10), 2138–2149 (2013).

Amir Nahas is graduated from the Ecole Superieure de Physique et Chimie Industrielles de Paris (ESPCI ParisTech) and Institut d'Optique Graduate School, two French engineering school specialize in physics and optics. He is currently working at the Institut Langevin (Paris, France) as a PhD student. His current research interests include full-field OCT (FF-OCT), with a focus on addition of the elastographic contrast to FF-OCT images.

Mickaël Tanter received the PhD degree in physics (acoustics) from the University of Paris VII in 1999. He is now a researcher in the CNRS and joined the Institut Langevin (Paris, France) in 2000. His current research interests include wave focusing techniques in heterogeneous media, medical ultrasonic imaging, ultrasonic brain imaging, shear-wave propagation in soft tissues for cancer detection, ultrasonic therapy, nonlinear acoustics, and active noise control.

Thu-Mai Nguyen graduated from the Ecole Superieure de Physique et Chimie Industrielles de Paris (ESPCI ParisTech), a French multidisciplinary engineering school, in 2009. She obtained her PhD degree at the Institut Langevin (Paris, France) in 2012. She is currently working at the University of Washington (Seattle, WA) as a postdoctoral fellow. Her research interests include shear wave elastography, with a focus on ophtalmic applications, and photoacoustic imaging.

Jean-Marie Chassot is a research engineer (CNRS, the French National Center for Scientific Research) with several years of experience in optical instrumentation. He graduated in the ENSICaen engineer school (master degree), and then worked for 6 years in the LMOPS (Optical Materials, Photonics and Systems Lab, University of Metz). He then joined the Langevin Institute in 2009, and supported scientists in developing OCT and photoacoustic setups and experiments.

Mathias Fink received the PhD degree in solid-state physics in 1970 and received the doctorat es-sciences degree in 1978 from Paris University. His current research interests include medical ultrasonic imaging, ultrasonic therapy; nondestructive testing; underwater acoustics; telecommunications; seismology; active control of sound and vibration; analogies between optics, quantum mechanics, and acoustics; wave coherence in multiply scattering media; and time-reversal in physics. He holds 28 patents, and he has published more than 300 articles.

A. Claude Boccara was dean of research at ESPCI-ParisTech. Among the optical methods he has developed new microscopies to increase depth and lateral resolution. Recently, ultimate measurements have found new fields of application going from detection of gravitational waves to 3-D imaging though scattering media. He has published more than 300 scientific articles (ISI/ Boccara A* or Boccara C) in international journals. In 2007 he founded the start-up LLTech devoted to medical imaging and diagnostics.